ACS APPLIED MATERIALS & INTERFACES

Research Article

www.acsami.org

Silver Deposition on a Polymer Substrate Catalyzed by Singly Charged Monodisperse Copper Nanoparticles

Jeong Hoon Byeon and Jeffrey T. Roberts*

Department of Chemistry, Purdue University, West Lafayette, Indiana 47907-2067, United States

ABSTRACT: Aerosol deposition of singly charged monodisperse copper nanoparticles was used to catalytically activate a polymer substrate for electroless silver deposition. An ambient spark discharge was used to produce aerosol copper nanoparticles, and the particles were electrostatically classified at an equivalent mobility diameter of 10 nm, using a nanodifferential mobility analyzer. Deposition of the copper particles onto the surface of the substrate was enhanced by thermophoresis. The copper-deposited substrate was then immersed in a Ag(I) solution, resulting in the electroless deposition of silver (~17 μm line width) on the previously deposited copper (~12 μm line width, using a shadow mask with a 100 μm in width patterned stripe). The arithmetic mean roughness and electrical resistivity of the silver pattern were 44.7 nm and 7.9 $\mu\Omega$ cm, respectively, which showed an enhancement compared to those from the nonclassified copper particles (roughness = 162.2 nm, resistivity = 13.3 $\mu\Omega$ cm), because of a more-uniform copper deposition.

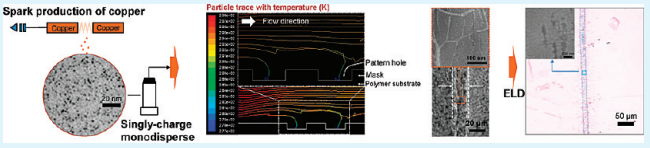

KEYWORDS: *aerosol deposition, singly charged, monodisperse copper nanoparticles, thermophoresis, electroless silver deposition*

INTRODUCTION

Silver and gold, while possessing excellent conductivity properties, are expensive materials. Copper and nickel display good electrical conductivity but are susceptible to ambient oxidation, resulting in the degradation of desirable properties.[1] In order to overcome problems associated with the high cost of silver or gold, or the oxidation of copper or nickel, the substitution of copper−silver films or patterns is currently considered to be an alternative option in electronics, catalysis, antimicrobial activity, and bioanalysis.[2−6] Several approaches have been established for fabricating bimetallic structures including chemical reduction, an electrochemical approach, and vacuum processes.[7−10] Among these techniques, electroless deposition (ELD) has been regarded as one of the most suitable processes, because of the advantages of simplicity and low cost.[9,11]

Inert substrates must be catalytically activated prior to ELD to provide a surface that can interact with metal ions in solution, enabling site-selective reduction and film growth.[12,13] The most commonly used ELD method employs wet tin-sensitization and palladium-activation steps. However, there are still major problems to commercialization, including impurities, high cost, and environmental pollution.[14−16] In order to circumvent this problem, Xu et al.[1] and Hai et al.[9] developed a procedure for making silver films through pretreatment with copper particles. However, these approaches still employ wet chemical steps. It would be advantageous to activate the substrate surface through simple, more effective, and more environmentally friendly means.[17] From this viewpoint, the present investigation demonstrates a silver micropattern on a polymer substrate by replacing the traditional activation with copper nanoparticles deposited from an aerosol, which does not involve expensive wet chemical and vacuum lithographic steps.

At the initial stage of electroless silver deposition, the catalytic particles (i.e., copper) serve as the anodic site at which the reductant can be adsorbed and oxidized. Formally speaking, the electrons released on oxidation travel through the copper particles and reduce ionic silver. The copper particles act as electron transfer carriers from the reducing agent to the silver ions, hence resulting in site-selective deposition.[18] Previous studies of aerosol activation reported that the deposition of catalytic particles affected the morphology of thin films and the quality of the patterns of electroless metal.[19−22]

In this paper, a silver micropattern was fabricated by producing singly charged monodisperse aerosol copper nanoparticles using a spark discharge[23] and a nanodifferential mobility analyzer (NDMA). Previous studies[20−22] have established that aerosol metal nanoparticles can be deposited onto polymer substrates by thermophoresis, which is a physical phenomenon in which aerosol particles move across a temperature gradient.[24] In order to enhance uniformity of aerosol deposition and economic feasibility regarding pretreatment, singly charged aerosol copper nanoparticles were deposited. This suppresses particle coagulation, because of a repulsive interaction between incoming and deposited particles, and subsequently enables a more-uniform electroless silver deposition.

METHODS

Process. Copper aerosol nanoparticles were produced via spark discharge and carried by nitrogen gas to a polymer substrate, as shown in Figure 1. In the experiments, polytetrafluoroethylene (PTFE) disks (pore size = 0.2 μm, diameter = 47 mm; No. 11807-47-N, Sartorius,

Received: February 8, 2012
Accepted: April 11, 2012
Published: April 11, 2012

   dx.doi.org/10.1021/am300217n | ACS Appl. Mater. Interfaces 2012, 4, 2515−2520

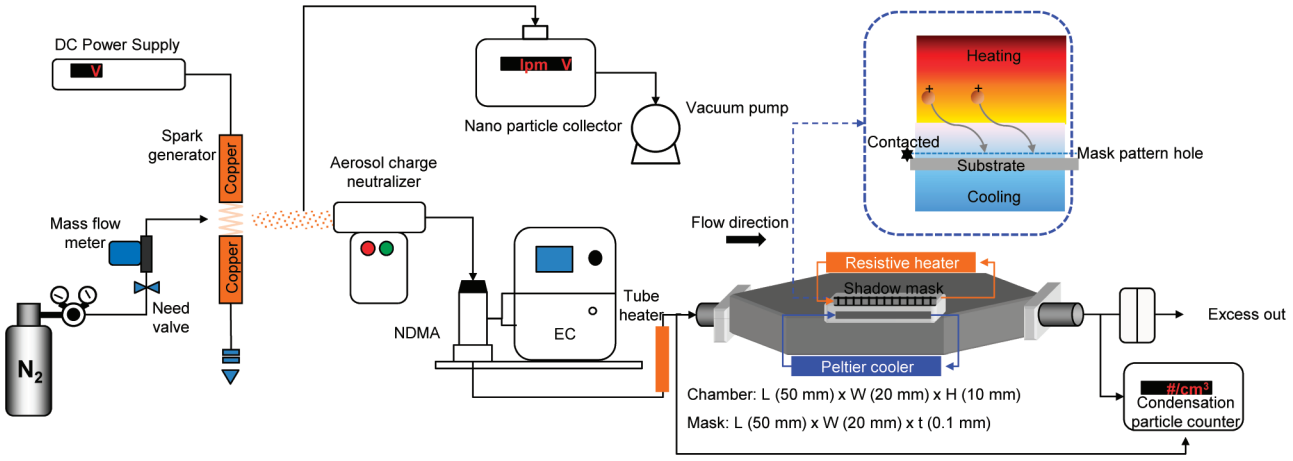

Figure 1. Schematic diagram of aerosol deposition apparatus used for this work.

Germany) having a thickness of 65 μm were used as the substrates. A spark was formed between two identical copper rods (3 mm in diameter, 100 mm in length; No. CU-112564, Nilaco, Japan) inside a chamber under a pure nitrogen environment (>99.99% purity) at standard temperature and pressure. The flow rate of the nitrogen gas was controlled by a mass flow meter with a precision needle valve (Model 3810DS, Kofloc, Japan). The electrical circuit specifications were as follows: resistance = 0.5 MΩ, capacitance = 1.0 nF, loading current = 0.3 mA, applied voltage = 3.4 kV, and frequency = 260 Hz. The produced particles were passed through an aerosol charge neutralizer (Model 4530, HCT, Korea), and injected into a nanodifferential mobility analyzer (NDMA) (Model 3085, TSI, USA). The NDMA was operated at a chosen fixed voltage provided by an electrostatic classifier (EC) (Model 3080, TSI, USA) to extract the particles of equivalent electrical mobility (Z_p). [Refer to eq 1, where p is the the number of elementary charge units, e the elementary unit of charge ($e = 1.6 \times 10^{-19}$ C), C_c the Cunningham correction factor, μ the gas viscosity, and D_p the equivalent mobility particle diameter.] Particles were classified at 10 nm, and the particle stream was directed into a thermophoretic deposition chamber.

$$Z_p = \frac{peC_c}{3\pi\mu D_p} \qquad p = +1 \text{ (positively singly charged)} \tag{1}$$

The NDMA was operated at an aerosol flow rate of 1.5 L/min and a sheath flow rate of 15.0 L/min, which created an aerosol-to-sheath ratio of 0.1.

The temperature of the particle-laden flow was maintained at 19 °C with a tube heater, and the temperature of the polymer substrate was maintained at −2 °C, thereby enhancing deposition of the particles onto the substrate via thermophoresis. Computational fluid dynamics (CFD) (Fluent 6.3, Ansys, USA, with a finite volume grid containing ~65 000 cells) calculations were performed with particle trajectories and temperature distribution in a thermophoretic deposition chamber. The particle trajectories were calculated using a Lagrangian formulation. Individual particle trajectories were tracked by solving the following force balance equations for each particle:

$$m_p \frac{du_p}{dt} = F_G + F_D + F_T \tag{2}$$

where u_p is the particle velocity, F_G, F_D, and F_T are the forces acting on the particle due to gravity, fluid drag, and thermophoresis, respectively. The thermophoretic force was calculated based on the equation proposed by Talbot et al.[25] and is expressed as

$$F_T = -\frac{6\pi D_p \mu_g^2 C_s (K + C_t Kn)}{\rho_g (1 + 3C_m Kn)(1 + 2K + 2C_t Kn)} \left(\frac{1}{T_g}\right) \nabla T \tag{3}$$

where μ_g is the gas viscosity, C_s, C_t, and C_m are dimensionless constants, K is the ratio of the gas and particle thermal conductivities, Kn is the Knudsen number, ρ_g is the gas density, and T_g is the gas temperature. Particle trajectories were calculated based on a fixed gas flow field obtained prior to the calculation of particle trajectories. The set of equations that govern for the gas flow were described by continuity, momentum, and energy equations for a compressible flow. Stochastic particle tracking incorporated the instantaneous values of the gas flow components in the particle trajectory calculations.

Temperatures were measured by an infrared thermometer (Model 42545, Extech, USA) and maintained by a resistive heater and a Peltier cooler. The substrate was then separated from the stainless steel shadow mask (Debora Electronics, Korea) and annealed at 240 °C for 10 min in pure nitrogen atmosphere to prevent the detachment of the particles from the substrate. After annealing, the copper-deposited substrate was immersed into an electroless silver bath, resulting in the deposition of silver on the copper nanoparticles of the substrate. The composition of the silver bath was 0.02 M (mol L^{-1}) of $(NH_4)_2$, 0.04 M of NH_4OH, 0.01 M of $AgNO_3$, 0.10 M of $C_4H_4O_6KNa$, and 0.01 M of HNO_3. The bath temperature was 45 °C. The proposed electrochemical half-reactions are as follows:[9]

$$Ag(NH_3)_2^+ + e \rightarrow Ag + 2NH_3 \qquad E^\circ = +0.373\ V$$

$$Cu + 4NH_3 - 2e \rightarrow Cu(NH_3)_4^{2+} \qquad E^\circ = -0.050\ V$$

The proposed net reaction is

$$Cu + 2[Ag(NH_3)_2]NO_3 \rightarrow [Cu(NH_3)_4](NO_3)_2 + 2Ag$$
$$\Delta E^\circ = +0.696\ V \tag{4}$$

During ELD, silver was deposited through redox chemistry involving the Ag-amine, as shown in eq 2. A comparison of the standard reduction−oxidation potentials ΔE° shown in eq 2 indicates that deposition of silver is thermodynamically favored. Silver nuclei that are formed on the surface of copper particles in the reaction act as the active sites for the further deposition of silver species. The substrate was rinsed with deionized water after it was removed from the bath to remove the residual and then was set aside to dry in a clean booth.

Instrumentation. Both size distributions of the nonclassified and classified aerosol copper particles were measured by a scanning mobility particle sizer (SMPS) system consisting of the NDMA, the EC, a condensation particle counter (Model 3776, TSI, USA), and the aerosol charge neutralizer (see Figure 1). The SMPS system was operated with a scan time of 135 s (with a measurement range between 2.02 nm and 63.8 nm).

After the particles were sampled on a carbon-coated copper grid located on a nanoparticle collector (Model NPC-10, HCT, Korea) 10 cm downstream of the spark generator, the morphology and microstructure of the copper particles were analyzed using a transmission electron microscopy (TEM) system (Model 3010, JEOL, Japan) operated at 300 kV.

Scanning electron microscopy (SEM) (NOVA nanoSEM, FEI, USA) images and energy-dispersive X-ray (EDX) (INCA 250, Oxford, U.K.) profiles for the samples were obtained at an accelerating voltage of 15 kV. A scanning probe microscopy (SPM) system (NanoScope IIIa, Veeco, USA) was used for the topography of the samples. The drive frequency was 330 kHz, and the voltage was between 3.0 V and 4.0 V. The drive amplitude was ~300 mV, and the scan rate was 0.5–1.0 Hz.

RESULTS AND DISCUSSION

Thermophoretic velocities were calculated according to the expression for the particles, with a Knudsen number of $Kn > 3$:

$$v_{th} = -\frac{3}{8}\left[\frac{\mu_g \nabla T}{0.499\rho_g T_g(1 + \pi\alpha/8)}\right] = -K_{th}\left(\frac{\mu_g \nabla T}{\rho_g T_p}\right) \quad (5)$$

where ∇T represents the temperature gradient in the vicinity of the particle, α is the accommodation coefficient, and K_{th} is the numerical coefficient estimated at $\alpha = 1$ ($K_{th} = 0.54$),[26] which increases with decreasing particle size. This considered the thermophoretic velocity for free molecular particles (eq 3), where the particle diameter is assumed to be much smaller than the gas mean free path. Equation 5 (variations of <10% over the velocity distributions) offered a reasonably accurate simple expression for predicting the thermophoretic deposition of particles. As shown in Figure 2, the particles were expected to be deposited on the polymer substrate by thermophoresis due to the temperature gradient. In Figure 3, while the temperature of the particle-laden flow was kept at 19 °C, the temperatures of the stainless steel mask (100 μm width × 100 μm depth for pattern, Debora Electronics, Korea) and polymer substrate were kept at 26 °C (to prevent the unwanted deposition of the particles onto the mask via thermophoresis) and −2 °C (to enhance the site-selective deposition of the particles onto the polymer substrate via thermophoresis) through the use of a resistive heater and a Peltier cooler, respectively.

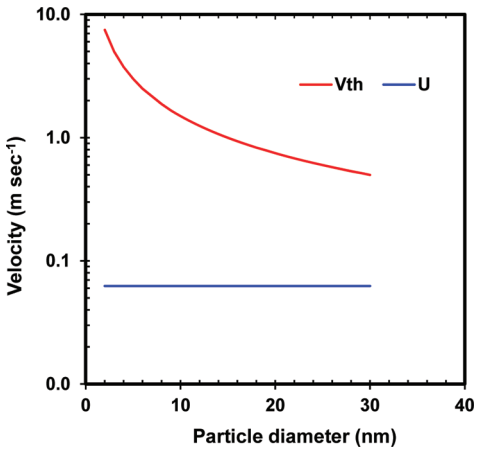

Figure 2. Thermophoretic velocity distribution as a function of particle size. U is the average upstream velocity of the particle-laden nitrogen gas flow.

The size distributions of the copper nanoparticles were measured using a SMPS, and the results are provided in Figure 4. The total number concentration, geometric mean diameter,

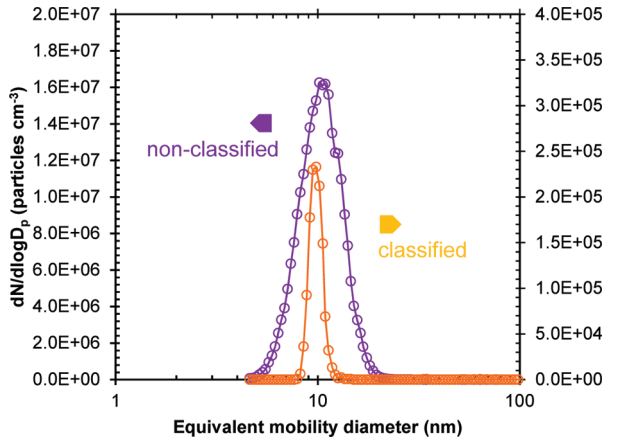

Figure 4. Size distributions of the spark-produced copper nanoparticles. The size classification of 10-nm copper particles was performed using a nano-differential mobility analyzer (NDMA).

and geometric standard deviation of the spark produced particles (i.e., nonclassified) are 4.26×10^6 particles/cm^3, 10.3 nm, and 1.27, respectively. The same data for the classified particles are 1.92×10^4 particles/cm^3, 10.0 nm, and 1.05, respectively. The morphology and structure of the particles were characterized via TEM and electron diffraction (ED). For the purposes of characterization, the size-classified copper nanoparticles were deposited on a carbon-coated copper grid. The TEM images (Figure 5) reveal that both the morphologies of the nonclassified and classified copper particles were agglomerates of several primary particles (each ~3.6 nm in diameter). The distribution uniformity of the classified case was greater than that of the nonclassified case, as expected. Figure 5 also shows the ED pattern corresponding to the TEM

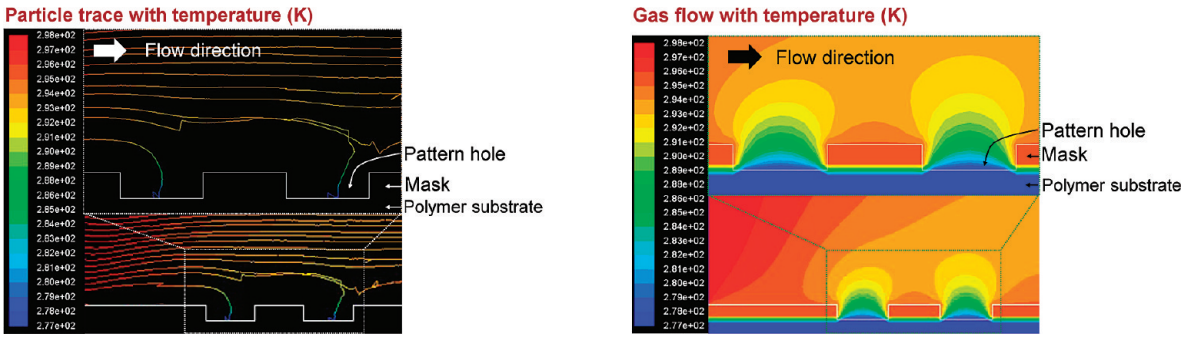

Figure 3. Computational fluid dynamics (CFD) calculations of the particle trajectory and temperature distribution in a thermophoretic deposition chamber.

dx.doi.org/10.1021/am300217n | ACS Appl. Mater. Interfaces 2012, 4, 2515–2520

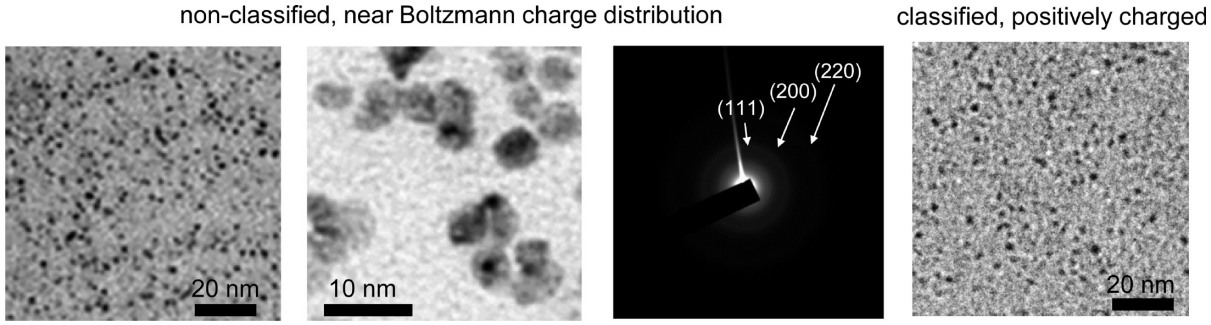

Figure 5. Transmission electron microscopy (TEM) images for the spark-produced copper particles, and the electron diffraction (ED) pattern.

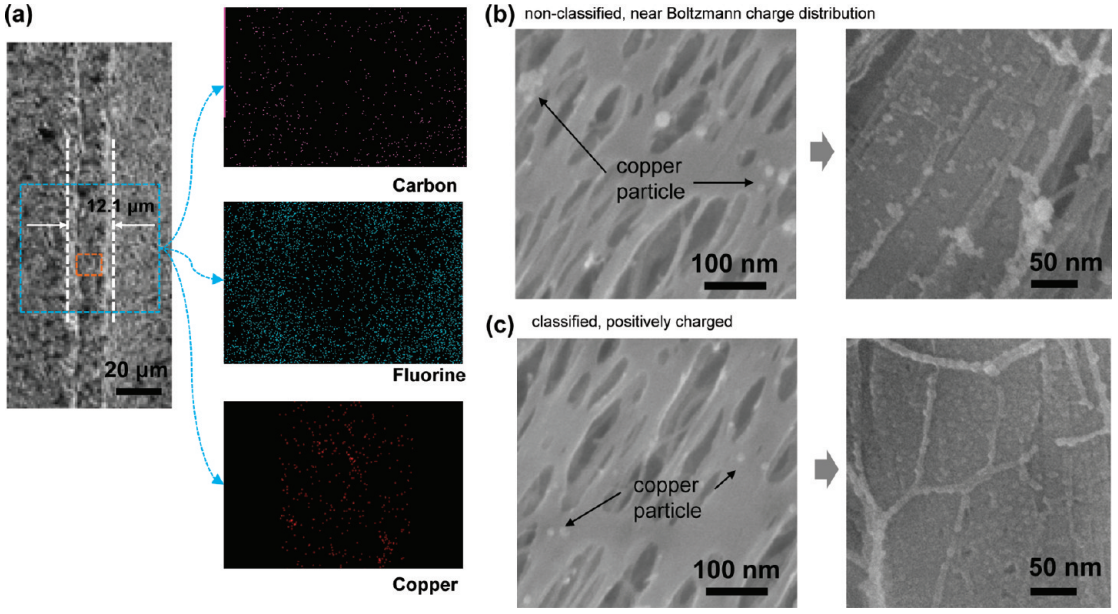

Figure 6. (a) SEM and EDX map images of the site-selectively copper-deposited polymer substrates (to be 1.12×10^{-2} mm^2 of copper per mm^2 of substrate). (b) SEM images of the nonclassified copper deposited polymer substrate. (c) SEM images of the classified copper-deposited polymer substrate.

micrograph. The pattern has a sharp diffraction line showing the (111) reflection and weak diffraction lines showing the (200) and (220) reflection of the face-centered cubic lattice for metallic copper, which indicated that the particles grew predominantly along the (111) lattice and mostly consisted of several nanometer-sized crystallites (~3.6 nm in this case). The deposition density (D_d) of a substrate with aerosol copper nanoparticles is defined as follows:[20,27]

$$D_d(D_p) = Qt_dA_s^{-1}m^{-1}\int_0^\infty \eta(D_p)C_a(D_p)\,dD_p \quad (6)$$

where Q is the flow rate of carrier gas (Q = 0.75 L/min), t_d the deposition time (1 min for nonclassified, 220 min for classified), A_s the plane area of the substrate, $\eta(D_p)$ the deposition efficiency ($\eta(D_p)$ = 0.394, measured by SMPS before and after the deposition chamber), and $C_a(D_p)$ the area concentration of copper particles. The deposition density on the polymer was selected to be ~1.12×10^{-2} mm^2 of copper per mm^2 of substrate.

Figure 6 shows SEM and EDX map images of the site-selectively deposited particles after annealing on polymer substrates. The SEM image for the classified case shows that the particles (~10 nm) are spread out over the entire surface with a gap, because of electrostatic repulsion before deposition.[28] The EDX maps for dotted area verify the copper particles only in a line of the pattern. The copper map shows that the particles were spread out over the entire line. The right-hand SEM image (another dotted area in the first image) for the classified case shows that the repulsive interaction due to the particle charges acted as a potential barrier, which suppressed the copper agglomeration nearly completely during deposition. The uniformity of the particle distribution for the nonclassified case was rather poor (GSD: 1.27) compared to that for the classified case (GSD 1.05). The first SEM image also shows that the thermophoretic focusing of the particles resulted in a line width of ~12 μm, which is much narrower than the width of the hole (100 μm) in the mask. As already shown in Figure 3, the particles were detached from the horizontal flow streamlines and mostly deposited on the central area of polymer substrates in good agreement with the experimentally determined results (Figure 6).

Figure 7a shows optical microscope images of the silver stripe patterns on the substrate from different copper size distributions (i.e., nonclassified and 10-nm classified). The silver patterns from both of the configurations of copper particles had a line width of ~17 μm. This may have originated from the same deposition conditions, such as the temperature gradient and the pattern dimensions. As shown in Figure 7a,

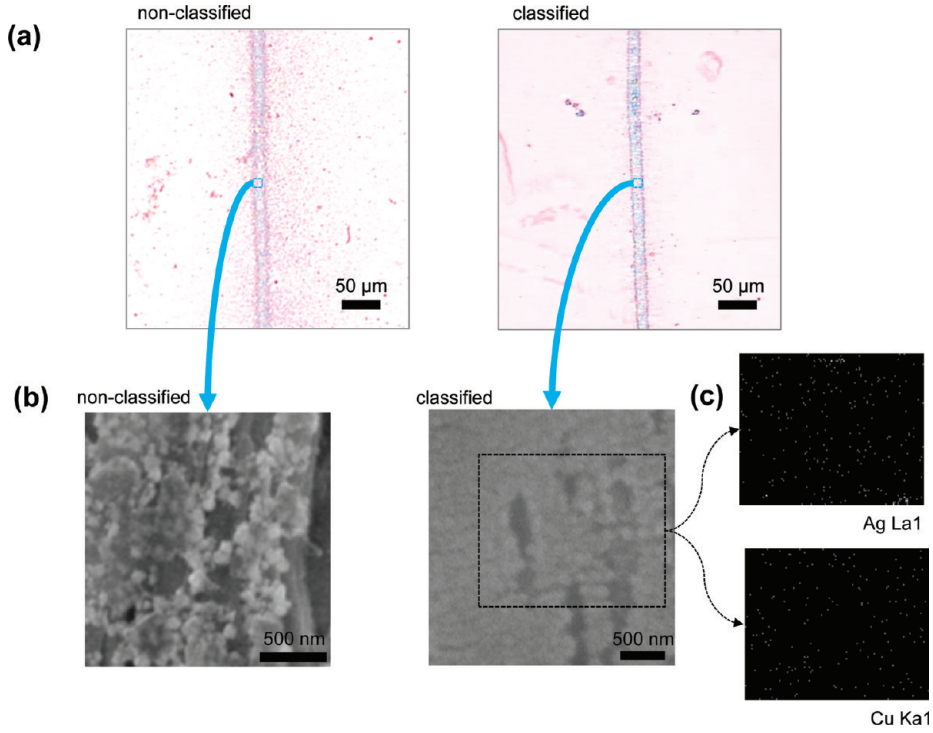

Figure 7. (a) Optical microscope and (b) SEM images of a silver pattern from nonclassified and 10-nm classified copper particles. (c) EDX maps for the dotted area in the SEM image (classified case).

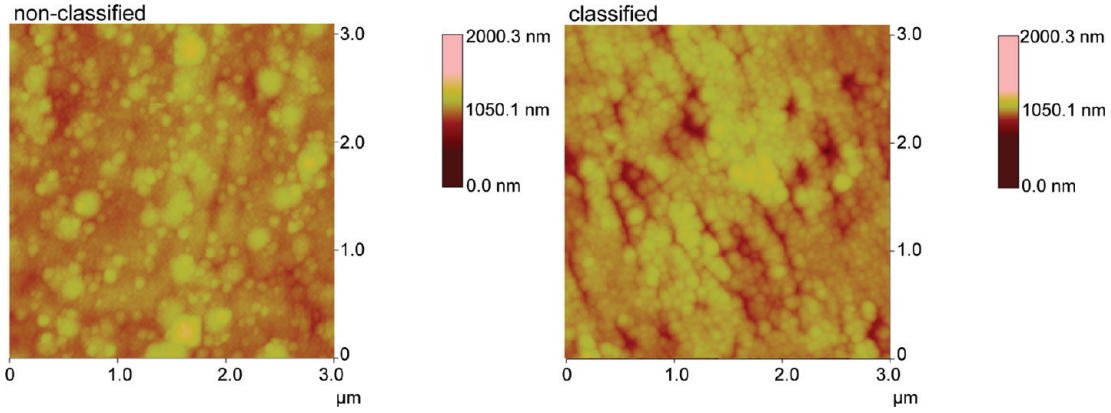

Figure 8. SPM topographs of the silver patterns from nonclassified and 10-nm classified copper particles.

the silver deposition occurred only on the copper particles, i.e., at the copper-deposited region of the substrate (Figure 5).[29] The copper particles effectively acted as seeds to initiate silver deposition. Hence, the process was clearly observed to occur by the initial nucleation at several sites on the substrate, followed by growth around these nucleated sites.[30] The line width of a silver pattern was wider than that of copper patterns (~12 μm, as shown in Figure 5), because ELD is an isotropic process. Figure 7b shows the SEM images of silver films (dotted areas in Figure 7a) from the different configurations of copper particles. Both silver stripe patterns show that silver particles were densely packed on the substrate, but their morphologies were quite different. A silver film from the classified case had a more uniform distribution of electroless silver particles. A report from Byeon and Kim[20] described that the uniformity of the electroless metal particles was largely influenced by the dispersion of seed particles (herein copper nanoparticles), and the nucleation resulted in particles formed directly on the top of the seed particles. EDX maps (Figure 7c) correspond to silver and copper, and the dots in these maps indicate the positions of each element in the dotted area in the SEM image (for the classified case).

Representative SPM images are shown in Figure 8, where the arithmetic mean thickness (and roughness) from the nonclassified and 10-nm classified copper particles were 1.04 μm (162.2 nm) and 1.11 μm (44.7 nm), respectively. It can clearly be observed that the classified case showed a more homogeneous coverage than the nonclassified case. A decreased uniformity of the nonclassified case on a polymer substrate was also described in previous study regarding substrate morphologies.[31] The substrate used in this study is same with one of the substrates used in the previous study.

Resistivities (ρ) of the silver pattern without sintering were calculated through the relationship $\rho = RA/L$, where R is the resistance, A the cross-sectional area, and L the length of the pattern. The average values of the resistivities for the

dx.doi.org/10.1021/am300217n | ACS Appl. Mater. Interfaces 2012, 4, 2515−2520

nonclassified and 10-nm classified cases were ~13.3 and ~7.9 $\mu\Omega$ cm, respectively. The value from the classified case is closer to the theoretical resistivity of bulk silver (1.6 $\mu\Omega$ cm), which may originated from a better uniformity of silver particles, compared to the classified copper particles.

CONCLUSIONS

The fabrication of a silver micropattern on the polymer substrate was performed using singly charged monodisperse copper nanoparticles. Spark produced copper nanoparticles were electrostatically classified to be a chosen size (10 nm), and were deposited onto the polymer substrate under a thermophoretic attraction between the particle and the substrate. The copper-deposited substrate was then immersed in an electroless silver bath, resulting in the deposition of silver (~17 μm line width) on the previously deposited copper (~12 μm line width) of the substrate. The arithmetic mean roughness and electrical resistivity of a silver pattern were 44.7 nm and 7.9 $\mu\Omega$ cm, respectively, which showed an enhancement, compared to those from the nonclassified copper particles (roughness = 162.2 nm, resistivity = 13.3 $\mu\Omega$ cm), because of a more-uniform copper deposition. Scaleup would be dependent on the rate of spark nanoparticle copper generation, and thus, an introduction of high-copper-number output systems may reduce time for silver pattern formation. The process was simple, cost-effective, and environmentally friendly, and can be applied in order to produce display electronic devices (sensors). It can also be applied to other fields, such as catalysis, antimicrobial material, and bioanalysis.

AUTHOR INFORMATION

Corresponding Author

*Tel.: (+1-765) 494-1730. Fax: (+1-765) 494-1736. E-mail: jtrob@purdue.edu.

Notes

The authors declare no competing financial interest.

ACKNOWLEDGMENTS

This work was partially supported by NSF Grant No. CHE-0924431.

REFERENCES

(1) Xu, X.; Luo, X.; Zhuang, H.; Li, W.; Zhang, B. *Mater. Lett.* **2003**, *57*, 3987.
(2) Kim, S. J.; Stach, E. A.; Handwerker, C. A. *Appl. Phys. Lett.* **2010**, *96*, 144101.
(3) Abbott, A. P.; Griffith, J.; Nandhra, S.; O'Connor, C.; Postlethwaite, S.; Ryder, K. S.; Smith, E. L. *Surf. Coat. Technol.* **2008**, *202*, 2033.
(4) Xiao, G.; Xian, C.; Li, H.; Chen, L. *J. Nanosci. Nanotechnol.* **2011**, *11*, 1923.
(5) Valodkar, M.; Modi, S.; Pal, A.; Thakore, S. *Mater. Res. Bull.* **2011**, *46*, 384.
(6) Su, Y.-T.; Lan, G.-Y.; Chen, W.-Y.; Chang, H.-T. *Anal. Chem.* **2010**, *82*, 8566.
(7) Tsuji, M.; Hikino, S.; Tanabe, R.; Matsunaga, M.; Sano, Y. *CrystEngComm* **2010**, *12*, 3900.
(8) Mancier, V.; Rousse-Bertrand, C.; Dille, J.; Michel, J.; Fricoteaux, P. *Ultrason. Sonochem.* **2010**, *17*, 690.
(9) Hai, H. T.; Ahn, J. G.; Kim, D. J.; Lee, J. R.; Chung, H. S.; Kim, C. O. *Surf. Coat. Technol.* **2006**, *201*, 3788.
(10) Misják, F.; Barna, P. B.; Tóth, A. L.; Ujvári, T.; Bertóti, I.; Radnóczi, G. *Thin Solid Films* **2008**, *516*, 3931.
(11) Hsu, C.-H.; Yeh, M.-C.; Lo, K.- L.; Chen, L.-J. *Langmuir* **2007**, *23*, 12111.
(12) Ng, J. H.-G.; Desmulliez, M. P. Y; Prior, K. A.; Hand, D. P. *Micro Nano Lett.* **2008**, *3*, 82.
(13) Srikanth, C. K.; Jeevanandam, P. *Appl. Surf. Sci.* **2009**, *255*, 7153.
(14) Aixiang, Z.; Weihao, X.; Jian, X. *Surf. Coat. Technol.* **2005**, *197*, 142.
(15) Schaefers, S.; Rast, L.; Stanishevsky, A. *Mater. Lett.* **2006**, *60*, 706.
(16) Tang, X.; Bi, C.; Han, C.; Zhang, B. *Mater. Lett.* **2009**, *63*, 840.
(17) Gong, J.; Lipomi, D. J.; Deng, J.; Nie, Z.; Chen, X.; Randall, N. X.; Nair, R.; Whitesides, G. M. *Nano Lett.* **2010**, *10*, 2702.
(18) Lee, C.-L.; Tseng, C.-M.; Wu, R.-B.; Syu, S.-C. *J. Electrochem. Soc.* **2009**, *156*, D348.
(19) Byeon, J. H.; Kim, J.-W. *Thin Solid Films* **2010**, *519*, 700.
(20) Byeon, J. H.; Kim, J.-W. *Langmuir* **2010**, *26*, 11928.
(21) Byeon, J. H.; Park, J. H.; Yoon, K. Y.; Hwang, J. *Langmuir* **2008**, *24*, 5949.
(22) Byeon, J. H.; Yoon, K. Y.; Jung, Y. K.; Hwang, J. *Electrochem. Commun.* **2008**, *10*, 1272.
(23) Byeon, J. H.; Park, J. H.; Hwang, J. *J. Aerosol Sci.* **2008**, *39*, 888.
(24) Gonzalez, D.; Nasibulin, A. G.; Baklanov, A. M.; Shandakov, S. D.; Brown, D. P.; Queipo, P.; Kauppinen, E. I. *Aerosol Sci. Technol.* **2005**, *39*, 1064.
(25) Talbot, L.; Cheng, R. K.; Schefer, R. W.; Willis, D. R. *J. Fluid Mech.* **1980**, *101*, 737.
(26) Fuchs, N. A. *The Mechanics of Aerosols*; Pergamon Press: Oxford, U.K., 1964.
(27) Byeon, J. H.; Kim, Y.-W. *ACS Appl. Mater. Interfaces* **2011**, *3*, 2912.
(28) Krinke, T. J.; Deppert, K.; Magnusson, M. H.; Schmidt, F.; Fissan, H. *J. Aerosol Sci.* **2002**, *33*, 1341.
(29) Moran, C. E.; Radloff, C.; Halas, N. J. *Adv. Mater.* **2003**, *15*, 804.
(30) Shankar, S. S.; Rizzello, L.; Cingolani, R.; Rinaldi, R.; Pompa, P. P. *ACS Nano* **2009**, *3*, 893.
(31) Byeon, J. H.; Kim, J.-W. *J. Electrochem. Soc.* **2011**, *158*, D15.